Science of the Total Environment 815 (2022) 152459

Contents lists available at ScienceDirect

Science of the Total Environment

journal homepage: www.elsevier.com/locate/scitotenv

Modeling the spatial and temporal variability in surface water CO_2 and CH_4 concentrations in a newly created complex of boreal hydroelectric reservoirs

Felipe Rust *, Pascal Bodmer, Paul del Giorgio

Groupe de Recherche Interuniversitaire en Limnologie, Département des Sciences Biologiques, Université du Québec à Montréal, Canada

HIGHLIGHTS

- Multiyear intensive study of CO_2 and CH_4 dynamics in three boreal cascade reservoirs.
- CO_2 and CH_4 drivers were reservoir morphometry, pre-flood landscape, and temperature.
- Drivers and seasonal trends differed for CO_2 and CH_4 and between reservoirs.
- Interannual trends differed between reservoirs, and between surface and deep layers.
- Proposed framework enables spatially cartography of CO_2 and CH_4 concentrations.

GRAPHICAL ABSTRACT

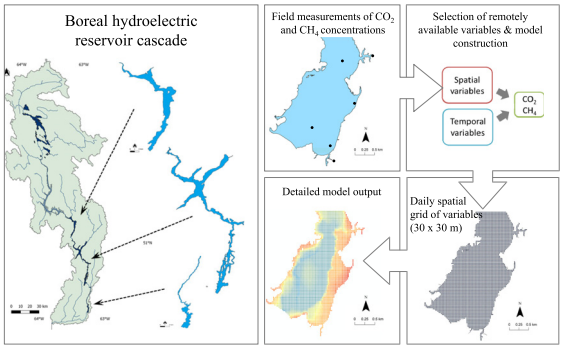

ARTICLE INFO

Article history:
Received 31 August 2021
Received in revised form 12 December 2021
Accepted 12 December 2021
Available online 21 December 2021

Keywords:
Greenhouse gas
Carbon
Dam
Hydropower
Diffusive emission
Reservoir cascade

ABSTRACT

Hydroelectric reservoirs emit carbon dioxide (CO_2) and methane (CH_4) to the atmosphere, yet there is still much uncertainty concerning the magnitude and drivers of these greenhouse gas (GHG) emissions. This uncertainty is particularly large over the initial years after flooding and in complex, cascade reservoir systems where studies are rare. We assessed the spatial and temporal patterns of CO_2 and CH_4 concentrations in the newly created La Romaine complex, which is composed of three consecutive reservoirs (RO1, RO2, RO3) along the La Romaine River. Dissolved CO_2 and CH_4 concentrations were intensively measured over three seasons for four years. Results show elevated CH_4 and especially CO_2 concentrations in surface waters of all three reservoirs upon flooding, with strong seasonality and high spatial heterogeneity within reservoirs. There was a strong seasonal decoupling of surface water CO_2 and CH_4 concentrations. Contrary to expectations, surface water CO_2 and CH_4 concentrations were relatively stable over the initial years of flooding, with exception of the decrease in CO_2 concentrations in the shallower RO1 reservoir. Further, individual reservoir characteristics, notably reservoir morphometry and pre-flood land cover, together with climatic factors were the main drivers of CO_2 and CH_4 concentrations, and the reservoir position in the cascade played a minor role. Models differed for CO_2 and CH_4, and also between reservoirs highlighting the need to capture these specificities in reservoir functioning. We establish a modeling framework to effectively fill the spatial and temporal gaps that inevitably exist in the sampling coverage of large and heterogeneous reservoirs, which combined with appropriately modeled gas transfer velocities, will serve as a platform to derive robust estimates of diffusive fluxes. This modeling framework can be transposed to other reservoirs, and will contribute to more accurate and representative estimates of diffusive carbon emissions from hydroelectric reservoirs.

* Corresponding author.
E-mail address: rustfelipe@gmail.com (F. Rust).

http://dx.doi.org/10.1016/j.scitotenv.2021.152459

1. Introduction

Hydroelectric reservoirs emit significant amounts of the two major greenhouse gases (GHG), carbon dioxide (CO_2) and methane (CH_4) to the atmosphere (Abril et al., 2005; Barros et al., 2011; Deemer et al., 2016; Fearnside, 2006; Kemenes et al., 2007; Rosa et al., 2006; Rudd et al., 1993). Over the past decade there has been an increasing awareness that these emissions associated with the creation of reservoirs for the generation of hydroelectricity and other uses need to be quantified and accounted for (Deemer et al., 2016). More recently, there have been calls to explicitly include reservoir emissions in carbon (C) inventories (IPCC, 2021), and to consider GHG emissions in the design and management of hydroelectric reservoirs (Almeida et al., 2019b). These developments highlight the need to improve the current estimates of reservoir GHG emissions, and the models used to predict future emissions (Prairie et al., 2018; Prairie et al., 2021). These emissions occur through three main pathways: (i) diffusive flux across the water-air interface (Roland et al., 2010; Teodoru et al., 2011), (ii) ebullition flux (bubbles) (Abe et al., 2005; Delsontro et al., 2010), and (iii) water degassing during turbine passage and in the downstream river (Guerin et al., 2006; Kemenes et al., 2007). The relative importance of the three pathways varies with reservoir size, morphometry, and geographic location (Harrison et al., 2021; Prairie et al., 2018), and each pathway has its own set of drivers and needs to be quantified, understood and modeled separately in order to improve the overall carbon footprint of reservoirs (Deemer and Holgerson, 2021).

One of the challenges when evaluating the overall carbon footprint of a reservoir is precisely to obtain accurate estimates of diffusive emissions, as these emissions are often highly variable in both space and time and they can vary by orders of magnitude even within a single reservoir. For example, diffusive emission of CH_4 varied spatially from 0.012 to 258 mg C m^{-2} day^{-1} in a tropical reservoir (Paranaíba et al., 2018), and a similar range was also observed in a boreal reservoir where CO_2 emissions ranged from 1760 up to 14,200 mg C m^{-2} day^{-1} (Teodoru et al., 2011). A recent global scale review (Deemer et al., 2016) showed that CH_4 fluxes (diffusive and ebullitive) across all types of reservoirs can vary up to 5 orders of magnitude. Multiple factors are involved in controlling both CO_2 and CH_4 concentrations and the resulting diffusive fluxes in reservoirs. Some of the variability in C emissions may be explained by the effect of extrinsic factors, such as regional climate, and the catchment characteristics (Mendonça et al., 2012). For example, temperature affects most processes involved in the production and consumption of CO_2 and CH_4 in aquatic systems. Both aerobic respiration and methanogenesis are temperature dependent (Chowdhury and Dick, 2013; Flanagan and Syed, 2011), but to a different extent (Sand-Jensen et al., 2007; Yvon-Durocher et al., 2014). Therefore, variations in temperature can lead to seasonal and inter-annual variability with higher C concentrations and emissions generally recorded in warmer months (Lima, 2005). Moreover, it has been shown that C concentrations and emissions are generally usually higher in reservoirs located in tropical areas (Barros et al., 2011), although this latitudinal effect was not observed in other studies (see e.g., Deemer et al., 2016). Variations in temperature can also be observed seasonally, although few studies show seasonal reservoir C concentration or emission data (Deemer et al., 2016; but see (Johnson et al., 2021). For example, in subtropical reservoirs diffusive CO_2 fluxes were higher in colder seasons (Wang et al., 2015; Wang et al., 2011) compared to warm seasons. Similarly, in a boreal reservoir, diffusive CO_2 emissions were higher in spring due to the winter CO_2 buildup under the ice cover, whereas diffusive CH_4 emissions were higher during summer due to higher water temperature (Bastien et al., 2011). Therefore, not taking seasonality into consideration may either under or overestimate annual-scale fluxes. Moreover, intrinsic factors play a key role in controlling the spatial heterogeneity in gas concentrations in the water column. Reservoir morphometry, for example, determines, among other things, the extent of contact between pelagic, littoral, and benthic areas, which strongly influence gas dynamics. Shallow littoral areas and riverine inflow areas tend to have higher CO_2 and CH_4 concentrations, and therefore higher emissions than the main reservoir channel (Paranaíba et al., 2018). In addition, a portion of the spatial variability of gas emissions can actually be explained by the composition of the pre-flood landscape in the different sectors of the reservoir, and this influence can last several years after flooding (Teodoru et al., 2011).

Hence, seasonality and differences in reservoir morphometry and in the pre-flood landscape often result in a large degree of both spatial and temporal variability in CO_2 and CH_4 concentrations in both surface and deep reservoir waters, and consequently in fluxes. This variability is exacerbated in reservoirs that have a large surface, have flooded watersheds with heterogeneous land cover and physiognomy, that have complex morphometries due to local topography, and that experience wide seasonal climatic shifts. In addition, the drivers of the production of CO_2 and CH_4 are not necessarily the same, and they are often only weakly coupled in time and space (Denfeld et al., 2020), such that each gas needs to be assessed separately. Thus, it is clear that in order to robustly determine the reservoir C emissions, it is essential to account for the heterogeneity in both gases (Paranaíba et al., 2018; Prairie et al., 2021). In this regard, previous studies have applied a range of sampling and reservoir upscaling approaches in order to address the issue of ambient gas heterogeneity, and Table S1 summarizes some examples. It is clear that sampling intensity, both spatial and temporal, varies greatly among studies, ranging from having a few discrete sampling points to a continuous sampling scheme at a fixed point, some considering seasonality while others do not (Table S1). This heterogeneity in approaches reflects in part the logistic challenges often encountered in the study of reservoirs, which are generally large and complex, often remote and with difficult access, all of which generally result in a limited spatial resolution and in compromises in terms of temporal coverage. Developing approaches that both maximize the spatial and temporal sampling coverage within the unavoidable logistical constraints, and which optimize the subsequent use of data is a key to reducing the overall uncertainty in current local and global estimates of reservoir C emissions (Deemer et al., 2016).

Here we present a large-scale study of dissolved gas concentrations (CO_2 and CH_4) within three reservoirs of the newly created La Romaine hydroelectric complex, the largest ongoing hydroelectric project in North America by installed capacity (Alicescu, 2021), composed of 4 consecutive reservoirs along La Romaine River in North Eastern Québec (Canada). The reservoirs are in a cascade configuration and in close proximity, they share the same water source (i.e., the La Romaine river) as well as the same basic climate features, regional chemistry, and hydrology, but they differ fundamentally in terms of morphometry and in the type of pre-flood landscape. This offered the rather unique opportunity of assessing how reservoir and pre-flood configuration influence the spatial heterogeneity and the seasonal and interannual patterns in CO_2 and CH_4 concentrations in each reservoir. In addition, we explored how the cascade configuration itself potentially influenced these patterns. We present the results of a 4-year study where we assessed both the spatial and temporal variability of CO_2 and CH_4 concentrations in the surface and deep waters of the three existing reservoirs over the initial years after flooding. On the basis of these observations we developed empirical models that link surface water gas concentrations to climate and remotely available variables, which provide both insight on the drivers and controls of gas concentrations in these reservoirs, and also tools to derive a spatially explicit cartography of gas concentrations that accounts for seasonality as well as for reservoir age. The latter is necessary in order to reduce the uncertainty involved in deriving fluxes from individual point measurements in highly heterogeneous reservoirs. Our overall objective was to model CO_2 and CH_4 concentrations in this newly created hydroelectric complex, which combined with appropriately modeled gas transfer velocities, will eventually yield more accurate and representative estimates of diffusive GHG emissions for these reservoirs and contribute to the development of robust overall C footprints for the entire complex. The modeling also increases our overall understanding of the drivers of both spatial distribution and of the temporal dynamics of these gases in these major boreal reservoirs.

2. Methods

2.1. Study site

The study was conducted in the La Romaine hydroelectric reservoir complex (Fig. 1 and Fig. S1). It is located in the La Romaine river (Strahler stream order 8) situated on the North shore of the Gulf of St Lawrence in the boreal Côte-Nord region in Québec, Canada. The reservoirs lie over the physiographic unit of the Laurentian Plateau (https://atlas.gc.ca/phys), this region is characterized by rocky hills, these steep stretches feature a series of waterfalls and rapids. There is negligible human land use within the watershed, which is characterized by approximately 82% natural forest, 10% wetlands, and 8% aquatic environments. This region is mostly covered by coniferous forest (45%), dominated by black spruce-moss, and secondarily by mixed stands (13.6%), broadleaf forest (3.6%), shrub (1.5%) and peatland (0.4%) (Hydro-Québec, 2008).

The La Romaine river, which is the major water source for all three studied reservoirs, drains a total area of almost 15,330 km^2 and travels nearly 500 km from the outlet of a chain of major headwater lakes to the Saint Lawrence River (Fig. 1). The characteristics of the river water vary little along its length; it is slightly humic, and moderately acid, iron-rich, and nutrient-poor and carries little suspended matter (Hydro-Québec, 2008). The ice cover starts forming in early December and starts to break in late-April, in the period from June and September the mean water temperature is around 14 °C. The regional mean annual air temperature is −2 °C and the annual mean precipitation is 940 mm (Hydro-Québec, 2008).

The current complex consists of four hydroelectric power plants that were commissioned between 2014 and 2021: La Romaine I (RO1; December 2015), La Romaine II (RO2; December 2014) and La Romaine III (RO3; May 2017). A fourth reservoir (RO4) was commissioned between 2020 and 2021, but is not included in this study. The total installed capacity is 1550 MW with an annual output of 8.0 TWh (www.hydroquebec.com/romaine/). The main characteristics of the three reservoirs studied here are summarized in Table 1 and Table S3.

2.2. Sampling design

In total, we performed 11 field campaigns between 2015 and 2018. For all sampling campaigns combined, samples were taken in 150 unique sites across all three reservoirs which were sampled several times over the studied period, for a total of 734 individual observations (305 in RO1, 378 in RO2, and 51 in RO3). To capture the seasonal variability of these systems, field campaigns were conducted over 20 days three times per year during the ice free period (May to November), in the months of June (spring), August (summer) and October (autumn), except in 2015, when only two campaigns were carried out (June and in August). Furthermore, in order to capture the spatial variability within the reservoirs and to retain the balance between shallow and deep regions, 45% of all investigated sites were located at the littoral (< 10 m deep), and 55% in the pelagic zone. Moreover, bottom water samples were taken using a Van Dorn bottle (Alpha™, WildCO, USA) in every campaign at the dam region in all reservoirs. In RO1 the deep samples were taken at 28 m depth and in both RO2 and RO3 at 60 m. The partial pressure of CH_4 and CO_2 (pCH_4 and pCO_2) in these deep samples was determined as explained below for surface water samples. Sampling of RO1 and the lower portion of RO2 was carried out by boat, whereas the upper portion of RO2, RO3 and the upper La

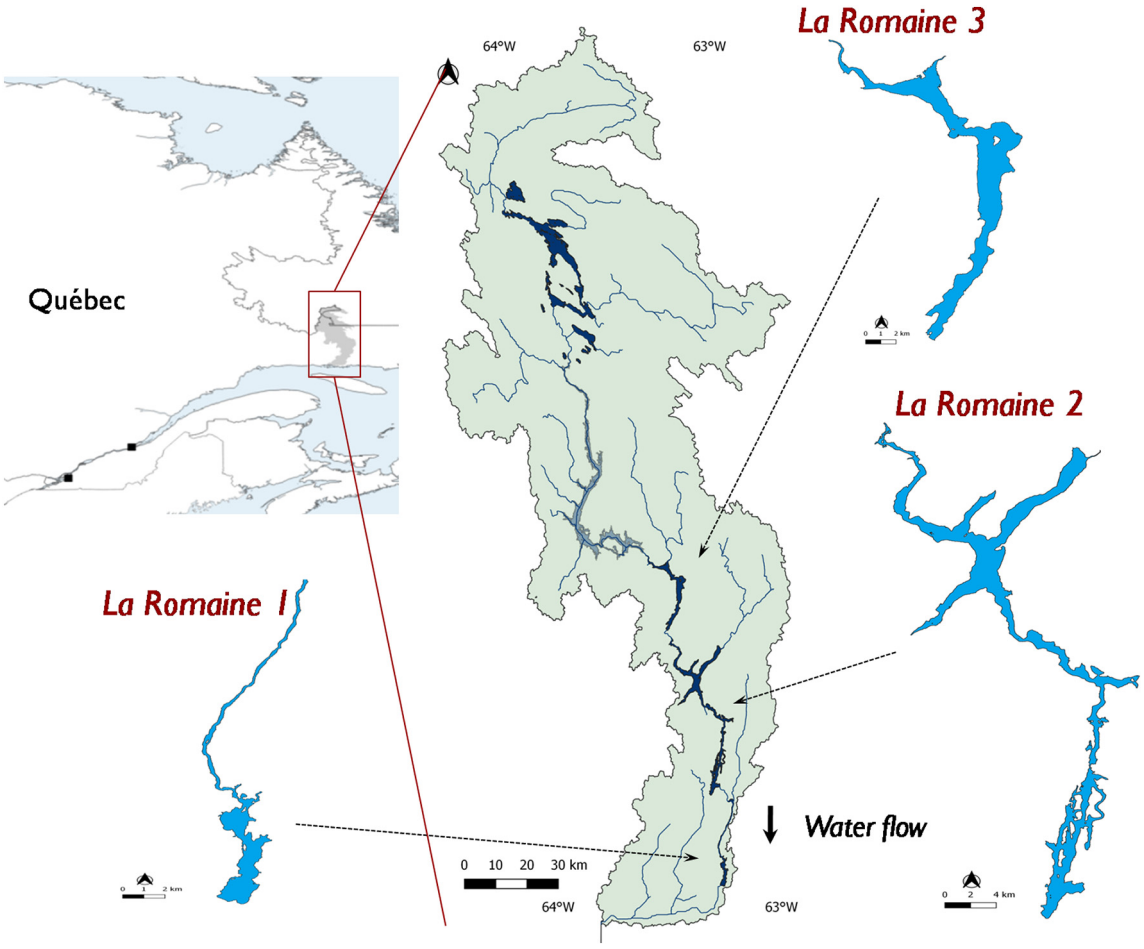

Fig. 1. Map of the geographical location of the sampling area, the La Romaine catchment, the main river and the location of three investigated reservoirs including their shape.

Table 1
Background information of the three sampled reservoirs with the year of installation in parentheses.

	La Romaine I (RO1 - 2016)	La Romaine II (RO2 - 2014)	La Romaine III (RO3 - 2017)
Dam height (m)	38	109	95
Turbine water intake (m)	19.5	45.4	37.4
Mean water depth (m)	22	61	67
Installed power (MW)	270	640	395
Catchment area	14.95 km^2	13.91 km^2	12.11 km^2
Residence time (days)	6	158	97
Position in the cascade	Most downstream	Center	Most upstream
Type	Run-of-river	Storage	Storage
Area (km^2)	12.6	85.8	38.6
[a]Water/Exposed land (%)	47.3	17.5	22.8
[a]Wetland (%)	1.0	0.1	0.0
[a]Bryoids (%)	3.9	1.0	0.0
[a]Shrub (%)	3.1	0.9	0.7
[a]Broadleaf (%)	6.7	3	0.4
[a]Mixedwood (%)	20.8	16.5	2.7
[a]Coniferous (%)	17.2	61	73.4

[a] Percentage of flooded land cover.

Romaine river sections were sampled by hydroplane. In addition to the discrete sampling, there was a floating autonomous measuring platform installed in the main channel of RO2 that yielded continuous surface water measurements of pCO_2 and pCH_4 for the ice free period, and there were systems installed in each of the three power stations taking continuous measurements of pCO_2 and pCH_4 of the water flowing through the turbine intake (see details in Section 2.4).

2.3. Environmental and limnological parameters

At each sampling site, surface water temperature (°C), conductivity (μS cm^{-1}), pH, and dissolved oxygen (O_2) saturation (%) were determined using a multiparameter probe (600XLV2-M, Yellow Springs Instruments, OH, USA). We also measured air temperature and wind speed at 1 m above the water surface with a handheld weather meter (Kestrel Meter 4000, PA, USA). In addition, surface water samples were collected using polypropylene bottles (5 L) at each sampling site for chemical analyses, which were processed the same day and stored refrigerated until analysis (see details in supplementary methods).

2.4. CO_2 and CH_4 concentrations

2.4.1. Discrete sampling and calculations

Samples to determine the surface water pCH_4 and pCO_2 were taken at each site using the headspace technique (Kling et al., 1991). We collected water in 1 L plastic bottles (Thermo Scientific™, Nalgene™ Square, USA) at 10 cm below the water surface, and removed 500 mL of water replacing it with zero air (AI 0.0UM, Praxair, Inc., Canada) using a peristaltic pump (Masterflex E/S Portable Sampler, USA) to create a headspace. Bottles were shaken for minimum two minutes to equilibrate the water- and air phases inside the bottle. The gas phase was then pumped back into an air-tight aluminum foil bag and pCO_2 and pCH_4 were measured in the same day in the field laboratory with an ultraportable greenhouse gas analyzer (UGGA, Los Gatos Research, Inc., USA). Both CO_2 and CH_4 concentrations were calculated by multiplying the respective gas partial pressure sampled at each site with the in situ temperature adjusted by Henry's law coefficient (Weiss, 1970; Wiesenburg and Guinasso, 1979).

2.4.2. Continuous gas measurements at turbine intake and float dock

Hydro-Quebec installed automated systems (Bastien et al., 2009) to measure continuously pCO_2 and pCH_4 at each reservoir generating station and one in a floating dock at the main channel in RO2 (Latitude: 50°31′ 31.2“ N, Longitude: 63°15’02.8”). pCO_2 and pCH_4 were measured in the water flowing through the turbines, which draw water from different depths depending on the reservoir (Table 1), and in the surface water of RO2 by the floating dock using a combination of a portable CO_2 (LI-820 CO_2 Analyzer, LI-COR, USA) and CH_4 analyzer (Panterra, Neodym Technologies, Canada). Each of the automated systems was connected to a water circulating system and a gas extraction module, the samples at the floating dock were taken at 0.5 m water depth. pCO_2 and pCH_4 was measured every three hours for the following periods: (1) RO1 from August 2016 to December 2018; (2) RO2 from February 2015 to December 2018; (3) RO3 from December 2017 to December 2018; (4) floating dock at RO2 from June 23 to October 15 in 2015, and from June 21 to October 16 in 2018.

2.5. Statistical analyses

We used regression tree analysis to identify and describe temporal and spatial patterns in CO_2 and CH_4 concentration among seasons as well as within and among the reservoirs. We used the rpart() function of the package ‘rpart’ (Therneau et al., 2019) to run the regression tree analysis. Linear regressions were performed to examine relationships between CO_2 and CH_4 concentrations in the three studied reservoirs and also between the measured CO_2 and CH_4 concentrations from the surface, bottom and turbine inlet. The reported R^2 values are adjusted for the number of data points. The significance of the regression slope was tested by analysis of variance (ANOVA) at a significance level (p) of 0.05. All modeling and statistical exercises were performed in R version 3.6.0 (R Core Team, 2018).

2.6. Modeling approach

2.6.1. Model development

We developed linear mixed effect models (LMM) to evaluate and predict the effects of spatial and temporal variables (Table S2) on the response variables CO_2 and CH_4 concentration in individual reservoirs using the lmer() function of the package ‘lme4’ (Bates et al., 2015). To facilitate the development of predictive models, especially in the case of this type of remote reservoirs with difficult access, we chose to develop the LMM using only remotely available variables (Table S2). We chose LMM because it has the advantage of fitting auto correlated (spatially and temporally) data (Bolker, 2015); site ID and field campaigns were considered as random effects.

Model selection was done using likelihood ratio chi-squared tests using the anova() function. First we built models containing all variables (full models) and compared these with reduced models in which we gradually dropped variables. Thus, variables that had no effect on response variables were removed. The selected model was then compared with a totally reduced model (without fixed effects) in order to validate whether it was statistically different. The final models were followed by a model validation, checking the residuals for normal distribution and homogeneity of variances. CH_4 concentration was log-transformed to improve normality and homoscedasticity of residuals.

2.6.2. Data preparation for modeling approach

For the spatial variables (Table S2), the sampled watershed was delineated using the *hydrology* tool (ArcGIS). The underlying land cover type (coniferous, broadleaf, mixed wood, shrub, wetland, exposed land, and water) was determined for each site for all the reservoirs using land cover maps (30 m × 30 m) obtained from GeoGratis (http://geogratis.cgdi.gc.ca/). Site depth was measured with a depth meter (Laylin Speedtech SM-5, USA). The closest distance from shore for each site was calculated using *near* tool (ArcGIS). All geospatial analyses were performed in ArcMap (version 10.1, Esri, USA). For the temporal variables (Table S2), the age of the reservoirs was calculated in decimal years from the flooding of each respective reservoir. Daily surface water temperature for the three reservoirs was modeled using the measured surface water temperatures using a polynomial regression based on a 42-day moving average of daily air temperature and the day of the year ($R^2 = 0.915, p < 0.0001$, Fig. S2); this approach provided the best fit to our observed water temperatures. The daily air temperature was obtained from a meteorological weather station located at 28 km from RO1, 48 km from RO2, and 96 km from RO3 (Latitude: 50°16′55“ N,

Longitude:63°36'41.0", https://climate.weather.gc.ca/). Average daily air temperature was calculated using hourly temperature measurements between the sunrise and sunset, since we sampled only during the day. We used getSunlightTimes function of the package 'suncalc' to retrieve sunrise and sunset times (Benoit and Achraf, 2019). We used modeled water temperatures in our LMMs rather than the measured water temperatures since the former are more integrative than our point temperature measurements, and consistent with subsequent spatial and temporal predictions of gases that we carry out in each of the reservoirs.

2.6.3. Model implementation

We used the empirical models described above to estimate the gas concentrations in areas and days that were not sampled. We generated a new dataset containing new georeferenced data points with all the model's fixed effects, over the ice-free period and across the entire surface of each of the three reservoirs. First, we created a georeferenced point grid using *fishnet* toolbox in ArcMap 10.1 (Fig. S3) covering all reservoir surfaces with the maximum resolution possible (same as the data set with the lowest resolution, i.e., land cover type, 30 m × 30 m), and as a result we generated 152,151 cells across the surface of all three reservoirs. For each of these cells we assigned a daily water temperature, a day of year, a reservoir age, a site underlying land cover type, a distance from the closest shore, and a maximum site depth, which was obtained from bathymetric analysis as the difference between before and after the flooding of the reservoirs, using a digital elevation model (resolution of 23 m × 23 m, obtained from GeoGratis). We then applied the corresponding reservoir empirical model to generate a daily value of CO_2 and CH_4 concentration for each cell based on the cell's properties using the prediction() function of the package 'lme4' (Bates et al., 2015).

3. Results

3.1. Temporal and spatial variability of measured CO_2 and CH_4 concentrations

The surface waters from all three reservoirs were consistently supersaturated in CO_2 and CH_4 relative to the atmospheric (Fig. 2). CO_2 and CH_4 concentrations were only very weakly correlated to each other (R^2 = 0.02, p = 0.0003), and varied over up to 3 orders of magnitude across all three reservoirs and in time (Fig. 2). The CO_2 concentrations ranged from

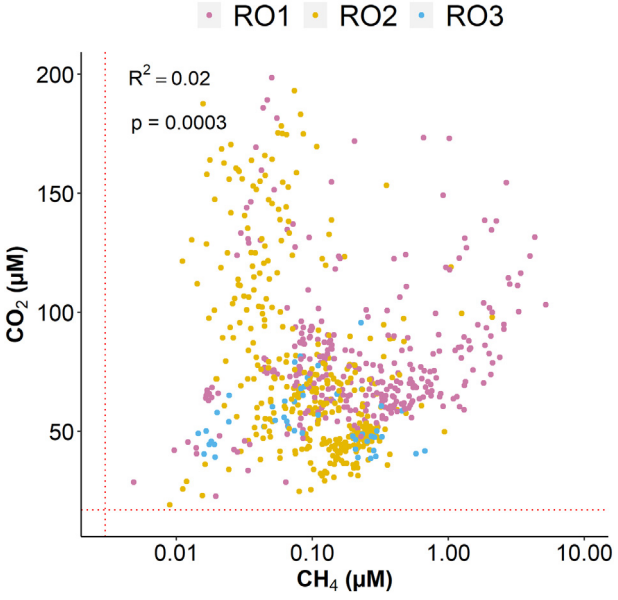

Fig. 2. Relationship between CO_2 and CH_4 concentrations in the three studied reservoirs. The dotted red lines indicate atmospheric CO_2 (18 μM) and CH_4 (0.003 μM) concentrations.

22 to 200 μM in RO1 (mean ± SD: 80 ± 29 μM), from 19 to 202 μM in RO2 (75 ± 38 μM), and from 39 to 95 μM in RO3 (58 ± 13 μM). The CH_4 concentration ranged from 0.004 to 5.2 μM in RO1 (0.5 ± 0.7 μM), from 0.007 to 2.1 μM in RO2 (0.1 ± 0.2 μM), and from 0.014 to 0.7 μM in RO3 (0.1 ± 0.1 μM).

There was a clear seasonal variation in the CO_2 and CH_4 concentrations in the sampled reservoirs (Fig. 3), significant differences in both CO_2 and CH_4 concentrations were observed between seasons ($p < 0.001$, Fig. S4). In general, CO_2 concentrations were on average highest in the spring (mean ± SD: 103 ± 44 μM), with a clear decrease towards the summer (60 ± 24 μM). In contrast, CH_4 concentrations were always highest in the summer (0.4 ± 0.6 μM), with the lowest average concentrations observed in the spring (0.2 ± 0.2 μM). Moreover, the upstream river followed a similar pattern of seasonal CO_2 and CH_4 concentration dynamics observed in the reservoirs (Fig. 3, upper panels), wherein CO_2 concentrations were slightly higher in the spring campaigns (40 ± 10 μM) compared with summer (27 ± 4 μM), and CH_4 concentrations were slightly higher in the summer campaigns (0.05 ± 0.03 μM) compared with spring (0.02 ± 0.01 μM).

A comparison of our point sampling of surface water CO_2 and CH_4 concentrations with the continuous sampling by the automated system deployed in the RO2 reservoir that measured surface CO_2 and CH_4 concentrations continuously, showed similar average values for the overlapping periods and over the seasons (Fig. S4). For example, the average CO_2 concentration over the summer measured in the platform was 54 ± 10 μM whereas the average in our sampling sites was 47 ± 9 μM (all sites included). For CH_4, the average concentration in the platform was 1.9 ± 1.6 and in our sampling sites it was 2.2 ± 1.0 μM.

CO_2 concentrations in the deeper layers of RO2 and RO3 were on average significantly higher than in the surface layer, which was not the case for the shallower RO1 (Fig. 4). In contrast, the CH_4 concentrations were similar between surface and deeper layers in all three reservoirs (Fig. 4). Moreover, there were generally no significant differences in both surface water CO_2 and CH_4 concentrations among the years sampled ($p > 0.05$, Fig. 3), except in RO1, where the average surface water CO_2 concentrations in 2018 (69 ± 20 μM) were significant lower (p = 0.001) than the average CO_2 concentrations in both 2016 (90 ± 38 μM) and 2017 (114 ± 26 μM). Interestingly, the deeper waters followed a different temporal dynamic than the surface waters in RO2, where the CO_2 concentrations measured at the turbine intake, representing a water mass between 35 and 45 m in depth, clearly decreased over the years (R^2 = 0.28, p = 0.008), as did the concentrations measured in comparably deep sites through discrete sampling (R^2 = 0.48, p = 0.002; Fig. 4). The concentration of CO_2 also declined in the deep layers of RO1 but paralleling the decline observed in surface water concentrations (Fig. 4). CO_2 also declined in RO3, but there are only 2 years of data, so the inter-annual trend was not clear established for this reservoir.

The three reservoirs differed in their average surface water CO_2 and CH_4 concentrations (Fig. S5). The average CO_2 concentrations over all sampling campaigns in RO3 (55 ± 13 μM) was significantly lower ($p < 0.001$) in comparison with CO_2 concentrations of both RO1 (81 ± 23 μM) and RO2 (75 ± 38 μM). In contrast, average CH_4 concentrations in RO1 (0.5 ± 0.7 μM) were significantly higher ($p < 0.001$) compared to RO2 (0.1 ± 0.01 μM) and RO3 (0.2 ± 0.1 μM). In addition, CO_2 and CH_4 concentrations varied spatially within each reservoir (see example in Fig. S6). The largest within reservoir CO_2 variability was observed during the spring season, ranging from 28 to 200 μM in RO1, 25 to 202 μM in RO2, and 51 to 95 μM in RO3 (Fig. 3). For CH_4 concentrations, the highest within reservoir spatial variability was observed in the summer, with values ranging from 0.01 to 4.3 μM in RO1, from 0.008 to 0.9 μM in RO2, and from 0.01 to 0.7 μM in RO3 (Fig. 3). In general, the spatial variability in CO_2 and CH_4 concentrations within reservoirs was related to the sampling location and to the pre-flood land cover underlying the sampling site, as evidence by the regression tree analysis (Fig. S7). In this regard, considering all reservoir data together, the regression tree analysis showed that sampling sites with less than 4.7 m in depth had higher average CO_2 concentrations (89 μM; n = 168) than deeper sites (74 μM; n = 570, p = 0.04; Fig. S7). A similar

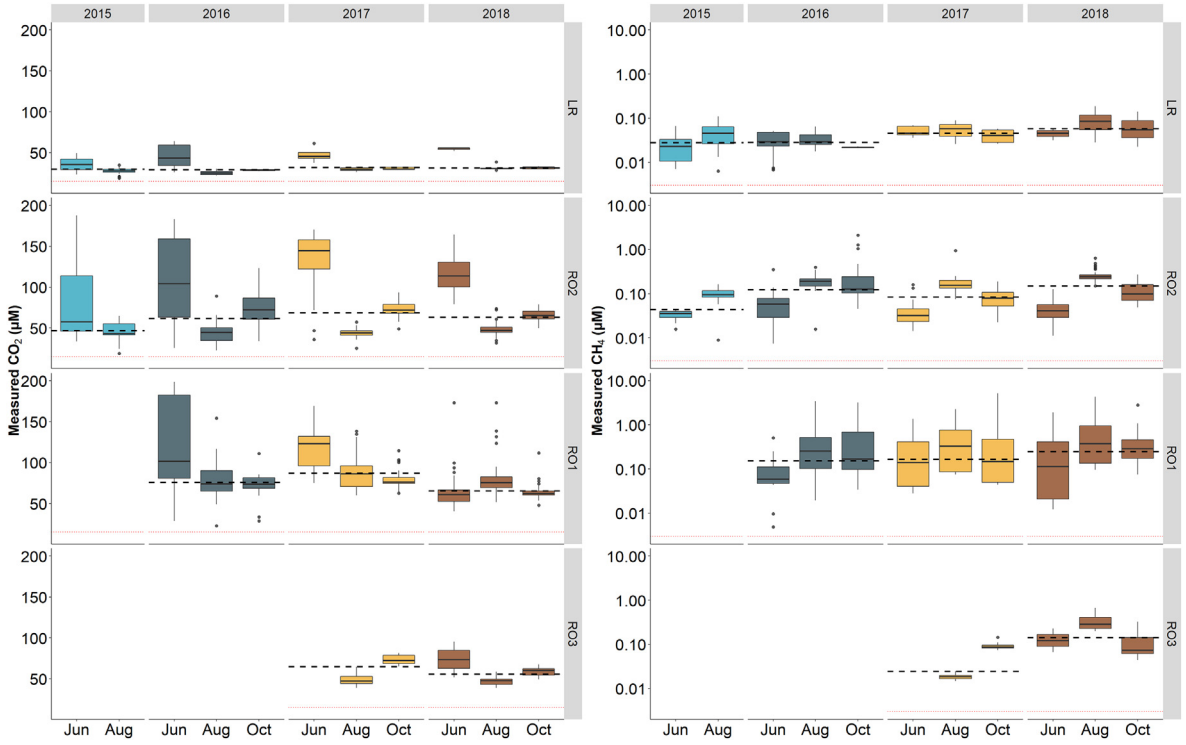

Fig. 3. Boxplots showing the temporal variability among sampled campaigns, reservoirs, and the La Romaine river (LR) of measured CO_2 (left) and CH_4 (right) concentrations. Boxplots represent median (black line), first and third quartiles (hinges), range (whiskers), and outliers (black dot). The dashed vertical lines represent mean annual concentrations of CO_2 and CH_4, respectively.

pattern was observed for sampling sites close to the shore (less than 69 m), which had higher average concentrations (83 µM, $n = 276$) than sites further offshore (74 µM, $n = 462$, $p = 0.02$; Fig. S7). Likewise, the same analysis for CH_4 concentrations also showed that shallower sites (less than 2.7 m, $p < 0.001$; Fig. S7) and sites closer to the shore (less than 30 m, $p < 0.001$; Fig. S7) had higher average CH_4 concentrations (0.98 µM, $n = 90$, and 0.75 µM, $n = 133$, respectively) than deeper sites and sites further offshore. The regression tree analysis also showed that sites underlain by wetlands had significantly higher CO_2 concentrations than all other sites in RO1 (109 µM, $n = 15$, $p = 0.004$; Fig. S8; others, 80 µM, $n = 293$), whereas sites underlain by broadleaf forest, mixed wood and shrubs had significantly higher ($p < 0.001$, Fig. S8) CO_2 concentrations (106 µM, $n = 62$) than all other sites in RO2 (71 µM, $n = 317$); RO3 did not show any dependency on pre-flood land cover. CH_4 concentrations showed significant dependency on pre-flood land cover only in RO1, and sites previously underlain by wetlands had significantly higher CH_4 concentrations that all other sites (1.7 µM, $n = 12$, $p = 0.004$; Fig. S8).

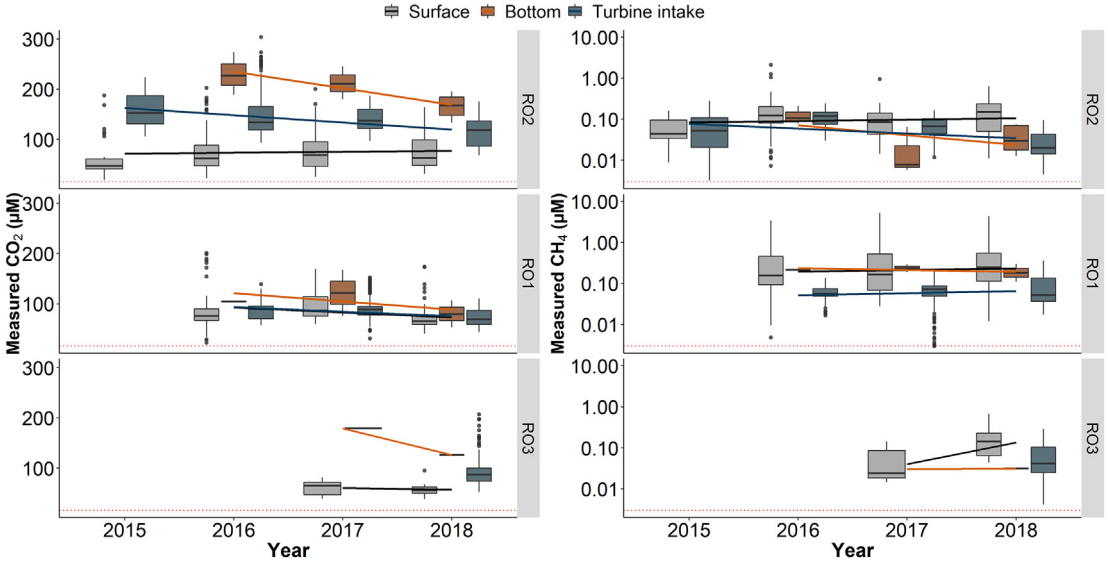

Fig. 4. Comparison of measured CO_2 (left) and CH_4 concentrations (right) of the surface, bottom and turbine intake of the three studied reservoirs. Boxplots represent median (black line), first and third quartiles (hinges), range (whiskers), and outliers (black dot). Lines represent linear regressions grouped by sampling site depth/location (colors of the lines match with the colors of the boxplots).

3.2. Effects of spatial and temporal variables on CO_2 and CH_4 concentrations

Considering the very weak relationship that was observed between the measured CO_2 and CH_4 concentrations (Fig. 2), it was necessary to build separate models for the two gases. For both CO_2 and CH_4 the models that combined all three reservoirs resulted in generally weaker model performance ($R^2 = 0.52$ for CO_2 and $R^2 = 0.70$ for CH_4, Table 2) compared to individual reservoir models (CO_2: R^2 0.59, 0.77, 0.66 for RO1, RO2, RO3, respectively; CH_4: R^2 0.83, 0.64, 0.67 for RO1, RO2, RO3, respectively, Table 2), and we therefore decided to pursue the latter for all subsequent analyses.

The models for CO_2 differed somewhat between reservoirs, for example site depth was selected in RO1 but not in RO2. Overall, day of the year, water temperature and site depth had a negative effect on CO_2 concentration (Table 2). In RO2 the interaction between day of the year and water temperature was more significant than both variables separately ($p = 0.01$). Reservoir age had a negative effect only in RO1, although this effect was borderline not significant ($p = 0.06$). Land cover type was selected in RO1 and RO2, albeit for different drivers: in RO1 sites underlain by wetlands had higher CO_2 concentrations, whereas broadleaf forest, mixed wood and shrub pre-flood land covers had a positive effect on CO_2 concentrations in RO2. The selected models for CH_4 were more similar between reservoirs compared to the ones selected for CO_2. We found a positive effect of water temperature and a negative effect of site depth on the CH_4 concentration in all reservoirs, and additionally in RO1, the pre-flood land cover ($p < 0.001$) was additionally selected (Table 2). The latter occurred due to presence of wetlands that had a positive effect on CH_4 concentrations.

3.3. Temporal and spatial variability of modeled CO_2 and CH_4 concentrations

We used the LMM in Table 2 to reconstruct daily CO_2 and CH_4 concentrations in each of the 30 × 30 m grid cells for the ice-free period, and thus generated an area-wide cartography of gas concentrations for each of the three reservoirs. The modeled CO_2 and CH_4 concentrations varied spatially within each reservoir, and followed a similar spatial pattern as the measured concentrations (Fig. S9). Overall, grid cells located over wetlands, broadleaf forest, mixed wood and shrub, and in shallow areas, had higher levels of both gases than the main channel of the reservoir (Fig. S9). The integrated reservoir CO_2 and CH_4 concentrations, which result from averaging the modeled concentration for all the grid cells within each reservoir, followed a clear seasonal pattern. High spring CO_2 values decrease towards the summer, with a subsequent CO_2 build up between summer and autumn in RO2 and RO3, whereas modeled CH_4 concentrations always peaked in the summer in all the three reservoirs, in agreement with our observations (Fig. 5). The magnitude of the modeled CO_2 and CH_4 differed between reservoirs, which is also in agreement with our observations (Fig. 5). On average modeled CO_2 was lower in RO3 (58 ± 9 μM) relative to RO2 (77 ± 13 μM) and RO1 (71 ± 18 μM), whereas modeled CH_4 was on average significantly higher ($p = 0.001$) in RO1 compared to in RO2 (0.09 ± 0.01 μM) and RO3 (0.11 ± 0.14 μM).

Table 2
Results of linear mixed models, testing effects of the spatial and temporal variables on CO_2 and CH_4 concentrations in each of the three reservoirs. Site ID and sampling campaings were included as a random effect on the intercept. Significance of fixed effects was assessed with likelihood ratio tests with degrees of freedom = 1. The slope direction (sign) of the effect is indicated with – or +.

Reservoir	Response variable	Fixed effect	χ^2	p	[a]R^2
All	CO_2	– Water temperature	26.5	<0.01	
		± Land cover type	20.4	0.04	
		– Reservoir	1.6	0.4	0.52
RO1	CO_2	– Day of the year	4.6	0.03	
		– Reservoir age	3.4	0.05	
		– Site depth	6.1	0.01	
		± Land cover type	10.2	0.03	0.59
RO2	CO_2	– Day of the year			
		– Water temperature			
		+ Day of the year × Water temperature	6.4	0.01	
		± Land cover type	10.7	0.09	0.77
RO3	CO_2	– Water temperature	5.4	0.01	
		– Site depth	2.3	0.12	0.66
All	log_{10} CH_4	+ Water temperature	4.2	0.04	
		– Site depth	4.2	0.03	
		± Land cover type	31.6	<0.01	
		– Reservoir	36.6	<0.01	0.70
RO1	log_{10} CH_4	+ Water temperature	12.4	<0.01	
		– Site depth	9.5	<0.01	
		± Land cover type	19.7	<0.01	0.83
RO2	log_{10} CH_4	+ Water temperature	6.7	<0.01	
		– Site depth	10.6	<0.01	0.64
RO3	log_{10} CH_4	+ Water temperature	4.4	0.03	
		– Site depth	7.3	<0.01	0.67

[a] Conditional R^2 considers the variance of both the fixed and random effects.

4. Discussion

Despite the growing awareness of hydroelectric reservoirs as GHG sources to the atmosphere at the global scale (Deemer et al., 2016) and the crucial role of adequate spatial and temporal assessments of CO_2 and CH_4 concentrations and emissions from reservoirs to determine accurate carbon budgets, few studies account and integrate the spatial and temporal variability of gas concentrations in these systems (Morales-Pineda et al., 2014; Paranaíba et al., 2018; Roland et al., 2010). We observed a large variability in surface water CO_2 and CH_4 concentrations within and among the three studied reservoirs and over seasons, but in contrast to other studies (Abril et al., 2005; Deshmukh et al., 2018), there was not a consistent pattern of decline in surface water gas concentrations over the initial years after flooding. Our modeling exercise of these concentrations reveals that the spatial variability may be attributed to the different pre-flooded land cover types and reservoir morphometry, and further that the drivers of CO_2 and CH_4 dynamics in the three reservoirs differ somewhat. In this regard, the modeling of spatial and temporal CO_2 and CH_4 concentration provides fundamental insight into the factors underlying C dynamics in these boreal cascade reservoirs. The fact that these models are exclusively based on remotely available variables is particularly useful because they provide effective tools for extrapolation and upscaling of these gas concentrations for the purpose of improving reservoir C footprint estimates.

4.1. Temporal and spatial variability in surface water CO_2 and CH_4 concentrations

4.1.1. Seasonal variability of measured CO_2 and CH_4 concentrations

The surface waters of the three reservoirs were consistently supersaturated in both CO_2 and CH_4 during the sampled period and hence were a constant source of CO_2 and CH_4 to the atmosphere (Fig. 2), and the range in CO_2 concentrations was in line with previous reports from boreal reservoirs (Demarty et al., 2009; Teodoru et al., 2011). We observed clear seasonal patterns in the surface CO_2 concentrations across the studied reservoirs, with highest CO_2 concentrations consistently occurring in spring and likely reflecting CO_2 accumulation under the ice cover during the winter months (Bastien et al., 2011). CO_2 degassing following ice thaw gradually decreased CO_2 concentrations in surface waters, which reached the lowest values during the summer. In autumn, CO_2 concentrations increased again in the deeper RO2 and RO3 reservoirs (maximum depths 120 m and 90 m, respectively) likely due to water column turnover and mixing with CO_2-rich hypolimnetic waters (Fig. 3). In contrast, the shallower RO1 reservoir (maximum depth 30 m) developed a much shallower and less stable hypolimnion, and therefore there was no autumn increase in surface CO_2 concentrations but rather a linear decrease in CO_2 concentrations from spring to autumn. These contrasting CO_2 seasonal patterns among reservoirs suggest that CO_2 dynamics are tightly related to reservoir morphometry, and that these seasonal patterns can differ markedly among reservoirs located close to each other and subjected to the same climate (Fig. 1).

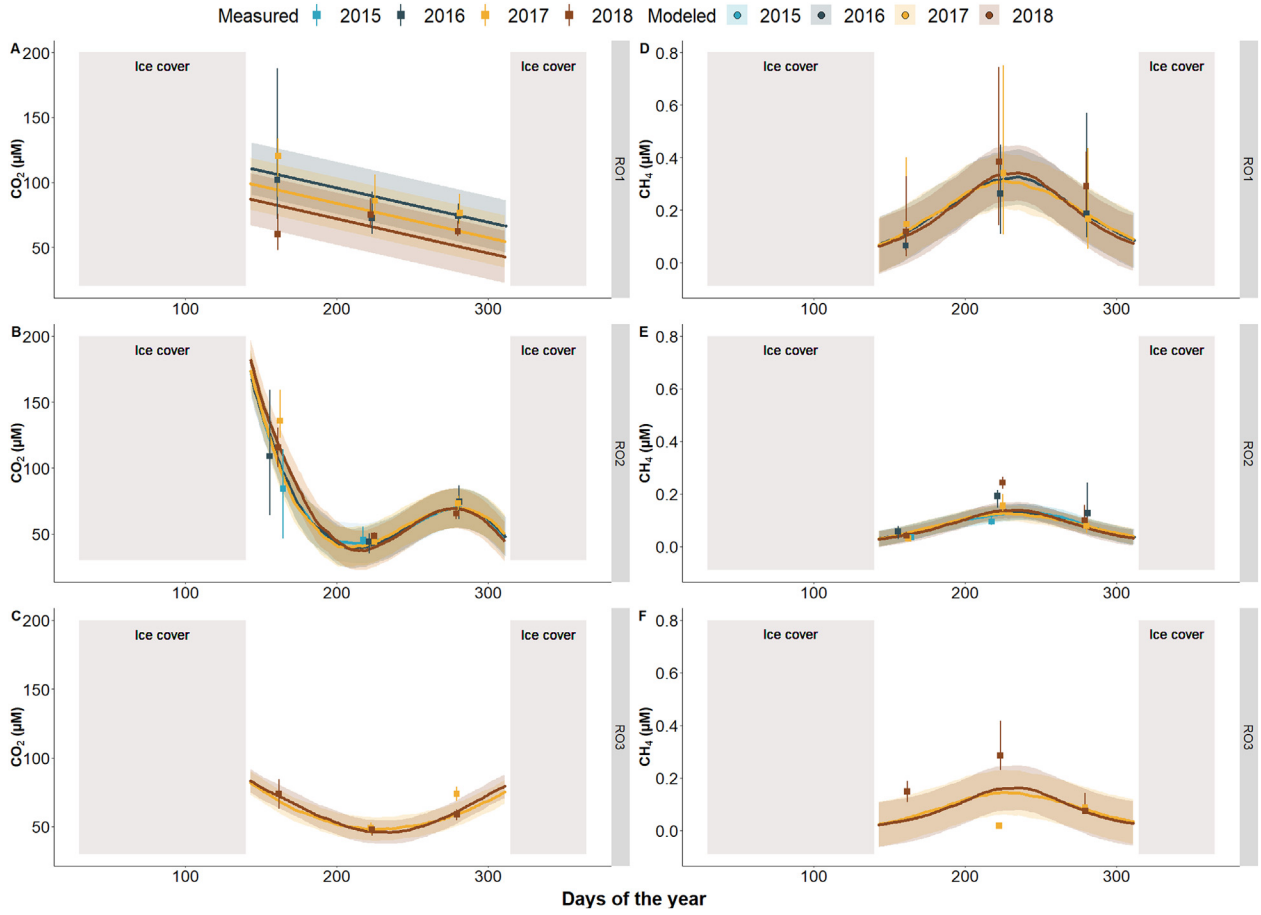

Fig. 5. Modeled concentrations of CO_2 (left) and CH_4 (right) over individual days in the ice free period. Each dot represents the modeled average of the CO_2 and CH_4 concentration in a day. Shaded polygons around the dots indicate 95% confidence interval for the mean. The squares and error bars represents the measured CO_2 and CH_4 concentration (median and inter quartile range) of each sampled campaign.

CH_4 concentrations were in general within the range reported for other boreal reservoirs (Demarty et al., 2009; Huttunen et al., 2002). Compared to CO_2, the CH_4 concentrations showed a more uniform temporal pattern among the reservoirs, with highest values consistently observed in the summer campaigns in all the three reservoirs, likely reflecting the strong dependency of CH_4 production on temperature (Yvon-Durocher et al., 2014). In contrast to CO_2, we did not detect high CH_4 concentrations in the spring after the ice melt, or after autumn overturn, and the continuous monitoring of CH_4 concentrations at the turbines (Fig. S10) did not reveal any significant CH_4 accumulation in deeper layers during winter. The absence of under ice CH_4 accumulation may reflect both low CH_4 production rates during winter due to low temperatures and perhaps CH_4 oxidation under the ice (Bastien et al., 2011).

Despite the importance of seasonality, very few studies have explored the temporal variability of both CO_2 and CH_4 concentrations and emissions in reservoirs, particularly in northern landscapes (but see e.g., Bastien et al., 2011, Demarty et al., 2011). In this regard, Wik et al. (2016) suggested that CH_4 emission estimates for northern lakes may be highly biased by short sampling periods, and reported uncertainties of around one order of magnitude associated to temporal overestimations or underestimations in CH_4 emissions. Our results also highlight the importance of seasonal sampling to obtain more accurate estimates of gas concentrations. For example, the average reservoir CO_2 concentrations would be overestimated by 75% if the sampling campaigns were carried out only during spring, whereas the CH_4 concentrations would be 4.5 times larger if the sampling campaigns were carried out only during the summer. Thus, omitting seasons in the sampling design leads to a bias of the annual reservoir carbon budget depending on the GHG measured. Further, the seasonal decoupling of surface water CO_2 and CH_4 concentrations is paramount to be considered in the sampling design of any future studies.

Recent studies have reported the importance of CO_2 and CH_4 emissions from drawdown areas in reservoirs where the water level varies significantly between seasons (Almeida et al., 2019a; Deshmukh et al., 2018; Keller et al., 2021; Kosten et al., 2018). However, in the three reservoirs studied here, the water level did not change substantially across the sampled seasons. For instance, the water level fluctuated by only 0.7 m in RO1 between 2016 and 2018 (details not shown), and therefore this aspect may not be as critical in these boreal reservoirs as it is in other regions.

4.1.2. Inter-annual trend of measured CO_2 and CH_4 concentrations

Previous studies have shown a clear negative relationship between CO_2 concentrations and reservoir age over the initial years after flooding (Abril et al., 2005; Teodoru et al., 2012a). For example, Teodoru et al. (2012a) showed a clear decrease in surface pCO_2 of over 50% over the first 4 years after flooding in a boreal reservoir, and a similar decline was also reported in a tropical (Abril et al., 2005) and in a subtropical reservoir (Deshmukh et al., 2018), and the most current models of reservoir CO_2 emissions involve declining functions with reservoir age (Barros et al., 2011; Prairie et al., 2021). This relationship, however, was not consistently found in the reservoirs studied here. RO1, the shallowest reservoir, was the only one which showed a significant decline in surface CO_2 over the first 3 years, with surface CO_2 concentrations in 2016 and 2017 being significantly higher than those found in 2018 (Fig. 3). In the other two deeper reservoirs, the surface CO_2 concentrations remained relatively stable over the first 4 years (RO2) and 2 years (RO3) post flooding. Interestingly, CO_2 concentrations within the deep layers in those two reservoirs showed a

different temporal pattern than in their respective surface layers. The deep samples and the automated measuring systems at the generating stations, which in both reservoirs draw water from layers between 35 and 45 m, showed a declining trend in CO_2 concentrations over the years (Fig. 4), which is in line with the decreasing inter-annual trend observed in other reservoirs (Abril et al., 2005; Deshmukh et al., 2018; Prairie et al., 2021; Teodoru et al., 2012b). The decoupling of surface and bottom layers is likely linked to reservoir morphometry and the depth of the water column. Reservoirs for which a declining trend in the surface CO_2 concentrations over the initial years after flooding has been reported are generally shallow. For example, the average depth of Nam Theun 2 reservoir (Deshmukh et al., 2018) is 8 m, while the average depth of Petite Saut reservoir (Abril et al., 2005) and Eastmain-1 reservoir (Teodoru et al., 2012a) is 11 m, and the RO1 reservoir (this study) is 22 m. On the other hand, the average depth of RO2 and RO3 reservoirs is 61 m and 68 m, respectively. In shallow reservoirs there is a closer contact with the flooded soils and a stronger coupling of surface gas dynamics with the ongoing degradation of the detrital terrestrial organic matter, with the resulting inter-annual trends of the surface CO_2 concentration. In deeper reservoirs, other surface sources and processes, such as lateral inputs from groundwater and tributaries, and pelagic metabolism may influence CO_2 concentrations, and may contribute to the stabilization of the surface concentrations on an inter-annual scale.

The contrasting inter-annual patterns of CO_2 dynamics in surface and bottom waters in these three reservoirs have major implications in terms of the distribution of C emissions in these systems, and how the contribution of the various pathways of emission to the total C footprint will evolve in time. Our results suggest that in the two deeper reservoirs, the surface diffusive emissions have remained relatively constant at least for the initial 4 years post flooding, whereas the downstream emissions at the turbine outlet have likely been declining over this period. In contrast, in the shallow RO1, both surface diffusive and downstream emissions may have been declining over the initial post-flood years.

Regarding the inter-annual variability of CH_4 concentrations, previous studies have shown an initial increase in the first years after flooding, followed by a decline (Abril et al., 2005; Venkiteswaran et al., 2013). The CH_4 concentrations in the water column of a tropical reservoir peaked one year after reservoir flooding and declined in subsequent years (Abril et al., 2005), whereas CH_4 concentrations increased through the first 3 years and declined slightly in the fourth and fifth year in small boreal reservoirs (Venkiteswaran et al., 2013). However, current reservoir GHG models do consider a stabilization of CH_4 concentrations after an initial increase in the first years (Prairie et al., 2021). In the studied reservoirs, we found slightly lower concentration values in the first year after the reservoirs were flooded and relatively stable concentrations over the following years (Fig. 3). This time lag in CH_4 concentration in the reservoirs may be linked to the slow development of anoxic bottom layers in these cold, deep boreal reservoirs, and the exogenous availability of alternative electron acceptors and labile OM, since the biogenic CH_4 is produced during the final step of anaerobic organic matter degradation when all other inorganic oxidants such as sulfate or ferric iron were already depleted (Conrad, 2009; Thauer et al., 2008). Overall, the longer term evolution of surface water CO_2 and CH_4 concentrations in these deep boreal reservoirs is difficult to predict a priori and will be a topic of future monitoring and research.

4.1.3. Variability of measured surface CO_2 and CH_4 concentrations among and within reservoirs

Although reservoirs are often built in a cascade configuration along river corridors, only few studies have assessed the spatial variability among reservoirs within a reservoir cascade configuration (Liu et al., 2020; Okuku et al., 2019; Shi et al., 2017; Wang et al., 2021). In a reservoir cascade in China (Mekong River), the upstream reservoirs (Gongguoqiao and Miaowei reservoirs) were found to be a hotspot of both CO_2 and CH_4 concentrations and diffusive emissions compared to downstream reservoirs (Shi et al., 2017; Liu et al., 2020), a pattern that which was linked to the higher sediment trapping that provided fresh organic carbon and enhanced mineralization. Previous studies also suggested a link between organic-rich sediment deposition and CH_4 production in reservoirs (Beaulieu et al., 2016; Maeck et al., 2013). Although we have not measured sedimentation in our study, La Romaine is a sediment-poor river, and we did not observe this link between the gas concentrations and potential sediment trapping in upstream reservoirs, and we did not find an effect of reservoir position. Rather, we attribute the average differences between reservoirs to differences in the pre-flood land cover and reservoir morphometry, factors which also determine the spatial heterogeneity of gases within each reservoir.

In this regard, several studies have highlighted the high degree of spatial variability of CO_2 and CH_4 concentrations that often occurs within reservoirs (Liu et al., 2020; Paranaíba et al., 2018; Soued and Prairie, 2020; Teodoru et al., 2011). For example, shallow and riverine inflow areas are likely to have higher concentrations of CO_2 and CH_4 than the reservoir main channel close to the dam (Paranaíba et al., 2018). Our results based on regression tree analysis showed that reservoir CO_2 and CH_4 concentrations were related to the location of the sampling sites (Figs. S6, S7, and S8). Sampling sites located over (i) specific pre-flooded land covers, and (ii) in shallow areas had higher concentrations of both gases than the main channel of the reservoirs. In particular, surface waters in sites overlying flooded wetland, shrub, mixed wood, and broadleaf forests had higher gas concentrations than surface waters in sites overlying flooded coniferous forest, potentially due to differences in organic matter content and composition of each flooded landscape type. It has been previously shown that pre-flooded land type influenced post-flood surface water CO_2 dynamics in a boreal reservoir (Teodoru et al., 2011) and this influence persisted for several years after flooding. Moreover, we observed higher levels of gas concentrations in shallower sites, thus water column depth can also be linked to the spatial heterogeneity in gas concentrations. As in our study, site depth has been linked to the spatial variation in pCO_2 in a tropical reservoir, where pCO_2 was higher in the shallow compared to deeper sites (Roland et al., 2010). Site depth could be a proxy to areas with increased contact to sediment metabolism, and also higher sedimentation rates, which could lead to higher CO_2 and CH_4 concentrations due to sediment organic matter degradation (Loken et al., 2019; Sobek et al., 2012). It is possible that the heterogeneity in gas concentrations reflects to some extent differences in gas exchange with the atmosphere, since sites close to the shore may be more sheltered than open sites and therefore have lower average gas exchange coefficients (Paranaíba et al., 2018), which would lead to higher average gas concentrations once other factors are accounted for. As we describe in the Section 4.2, we did not explicitly include gas exchange as a predictor variable in our modeling of gas concentrations.

4.1.4. Modeling CO_2 and CH_4 concentrations with remotely available variables

Our results suggest that although the three study reservoirs are subject to a similar climate, and in close proximity to each other, there are differences in C gas dynamics and in the underlying drivers. The mixed effect models allowed us to identify the main temporal and spatial variables driving surface water CO_2 and CH_4 concentrations in the individual reservoirs. Water temperature had a negative effect on CO_2 concentrations in RO2 and RO3 despite the known positive dependence of microbial activity and heterotrophic respiration on water temperature (Sand-Jensen et al., 2007; Yvon-Durocher et al., 2014). CO_2 concentrations were higher in June (spring) and October (autumn) when temperatures are much lower compared to August (summer). This relationship, however, does not reflect metabolism, but rather patterns in CO_2 accumulation within the system. Thus, in June, CO_2 concentrations were likely driven by CO_2 accumulation under ice and subsequent thawing rather than due to increased microbial metabolic activity. In October, CO_2 concentrations were likely driven by CO_2 input from the hypolimnion, since RO2 and RO3 were thermally stratified during summer and mixed in autumn (Fig. 3). Similarly, the day of the year in which the samples were taken also had negative effect CO_2 concentrations, but only in RO1 and RO2. As for water temperature, the day of the year seems to be a proxy for the higher CO_2 input from ice cover and snow thaw during June. Thus, our results show that the seasonal variability of CO_2 concentrations in boreal reservoirs seems to be tightly coupled to

reservoir morphometry, patterns of water column stratification and the ice regime within the reservoir and surrounding catchment, as has been recently pointed out (Deemer and Holgerson, 2021; Wang et al., 2021). In contrast, water temperature had a positive effect on CH_4 concentrations in all three reservoirs, showing the expected relationship between CH_4 production and temperature (Yvon-Durocher et al., 2014). Our findings underline the importance of water temperature in predicting the variability of surface water CH_4 concentrations, seasonally within reservoirs as we show here and in agreement with recent studies (McClure et al., 2020), but also across reservoirs along latitudinal gradients (Barros et al., 2011).

Spatially, site depth and pre-flooded land cover were the strongest predictor variables to model the spatial patterns in gas concentrations. For example, depth and pre-flooded land cover had an effect on CO_2 concentrations in RO1, which may reflect a combination of several processes. On the one hand, higher concentrations were observed in the shallow channel (average depth of 3.5 m) that connects RO2 to RO1, where RO1 receives CO_2-rich hypolimnetic water from RO2, yet this CO_2 is basically all degassed before reaching the lacustrine zone of RO1. This represents a legacy effect of the upstream reservoir on RO1 gas dynamics, as part of the complexity of the cascade configuration. On the other hand, highest concentrations of CO_2 were typically found over shrub, and wetlands land covers, which were also relatively shallow areas (average depth of 4.8 m). In contrast, site depth was not selected in RO2, and only land cover had a significant effect on CO_2 in this reservoir. Highest CO_2 values were found associated to the two specific land covers, mixedwood forest and shrub, which are found further south of the reservoir, near the dam. This area is particularly deep, thus the general negative effect of water column depth on CO_2 was not observed in RO2. In contrast, site depth had a negative relationship with CH_4 concentrations in all the three reservoirs. Furthermore, in RO1, land cover had a strong influence in the CH_4 concentrations. In particular, sites overlying mixed wood, shrub land and wetland types had on average 2 to 6 times higher CH_4 concentrations than other land covers, highlighting the importance of the pre-flood land cover on the C dynamics of the reservoir (Fig. S11).

Previous studies have identified trophic status, as reflected in nutrient or chlorophyll concentrations, as major predictors of GHG concentrations and fluxes in reservoirs worldwide (Deemer and Holgerson, 2021; DelSontro and Downing, 2018; Harrison et al., 2021). Overall, chlorophyll and nutrients (TP and TN) were not significant drivers of CO_2 and CH_4 in our three reservoirs (Fig. S12). There was a weak positive relationship between TP and pCO2 ($R2 = 0.15$, Fig. S12), which is in itself rather counterintuitive and perhaps reflects the fact that shallow reservoir sites tended to have higher pCO2 and also more TP from sediment remobilization (Fig. S12). Nutrients or chlorophyll have not emerged as major drivers across boreal reservoirs in general, likely because these systems tend to be consistently oligo- to mesotrophic, and never reach the threshold of enrichment where CO_2 and especially CH_4 dynamics become dominantly driven by eutrophication. Rather, reservoir morphometry, pre-flood landscape, and temperature / ice regime appear to be main drivers of CO_2 and CH_4 dynamics in these boreal reservoirs.

4.2. Implications to modeling reservoir GHG emissions and estimating the reservoir C footprint

Hydroelectric reservoir diffusive GHG emissions are often highly variable in both space and time, for example diffusive CH_4 emissions can vary globally up to 5 orders of magnitude (Deemer et al., 2016). Improving CO_2 and CH_4 emission estimates from reservoirs has been identified as one of the top priorities in the coming decades, both in terms of their net C footprint (Prairie et al., 2021) and in terms of their contribution to the global C balance (DelSontro and Downing, 2018; Rosentreter et al., 2021). Although CO_2 and CH_4 concentrations are not a direct measure of emissions, they are the most important factor influencing the magnitude and heterogeneity of these emissions (Morales-Pineda et al., 2014; Paranaíba et al., 2018; Sobek et al., 2005), and therefore understating and effectively modeling gas concentrations is key to deriving robust diffusive reservoir emissions. Here, we used temporal and remotely available spatial variables (Table S2) and developed spatial and temporal integrated empirical models to predict CO_2 and CH_4 concentrations in these three connected reservoirs. This modeling approach is key to filling in the spatial and temporal gaps that inevitably exist in the sampling coverage of large and heterogeneous reservoirs, especially those which, like La Romaine complex, are remote and of difficult access. The models that we developed here allowed us to generate a spatially explicit cartography of CO_2 and CH_4 on a 30 m × 30 m grid for each of the three reservoirs, and to project this cartography on a daily basis along the open water period and over 4 years. Beyond allowing us to explore the main drivers of gas dynamics in these reservoirs, and to derive a robust perspective of daily average gas concentrations for each reservoir that effectively accounts for spatial heterogeneity, this modeling framework will serve as a platform to derive robust estimates of diffusive fluxes for each of the reservoirs. In this regard, we are currently working on modeling gas exchange (k) in these reservoirs as a function of wind speed, reservoir location, and depth, using a database of hundreds of chamber-based measurements carried out in these sites (Bodmer et al. in prep). We can then overlay the resulting empirical models of k_{CO2} and k_{CH4} upon the same spatial grid as for the modeled concentrations, run at hourly time scales using locally modeled wind, and combine these modeled k estimates with the modeled gas concentrations. Consequently, we derive a detailed cartography of diffusive CO_2 and CH_4 emissions that accounts for both the drivers of gas concentrations and the heterogeneity of physical forcing, and that further accounts for temporal variability in both components. This detailed emission cartography, and the resulting temporal patterns in GHG emissions, would be impossible to reconstruct on the basis of propagating discrete measured seasonal mean flux values, a challenge that is not unique to La Romaine, but that is faced in most reservoir studies that have to make either spatial, temporal, or most often spatial and temporal compromises (see Table S1 for examples). This same georeferenced grid can subsequently be used to model other components of the C footprint of the reservoirs that also have an explicit location / morphometry dimension, such as ebullitive CH_4 fluxes, drawdown effects, and plant-mediated fluxes, all at the same spatial resolution, and within the same coherent framework. Beyond the effectiveness of this approach as a key element in determining a robust C footprint for La Romaine reservoir complex, we propose this as a useful framework for reservoir studies in general, where access and limited resources constrain the spatial and temporal sampling coverage in systems that are often large and highly heterogeneous.

CRediT authorship contribution statement

Felipe Rust: Conceptualization, Writing – original draft, Formal analysis, Visualization. **Pascal Bodmer:** Conceptualization, Writing – review & editing. **Paul del Giorgio:** Supervision, Conceptualization, Writing – review & editing, Funding acquisition.

Declaration of competing interest

The authors declare no competing interests.

Acknowledgements

The authors thank Serge Paquet, Alice Parkes, Annick St-Pierre for coordinating the field and lab operations, and the members of the CarBBAS team who contributed to the field campaigns and sample processing over the course of the years: Trista Vick-Majors, Clara Ruiz-Gonzalez, Erin Hotchkiss, Marie Geraldin, Karelle Desrosiers, Masumi Stadler, Martin Demers, Joan Pere Casas-Ruiz, Mathilde Couturier, Sophie Crevecouer, Sarah Mercier-Blais and all the undergraduate student interns who over the course of the years contributed to this project. We are also very grateful to Vincent Fugère, Yves Prairie, Paula Reis, and to Ryan Hutchins for discussions, and to Pierre Desjardins for guidance and wisdom in the field. We acknowledge Maude Demarty and Charles Deblois (Aqua-Consult) for

collecting and providing the continuous gas data, and Alain Tremblay and François Bilodeau (Hydro Quebec) for allowing the use of the data and for their continued and critical support with field logistics, operations and safety. This study is part of the program of the Carbon Biogeochemistry in Boreal Aquatic Systems (CarBBAS) Industrial Research Chair, co-funded by the Natural Science and Engineering Research Council of Canada (NSERC), and Hydro-Québec. We thank two anonymous reviewers for constructive inputs that improved the manuscript.

Appendix A. Supplementary data

Supplementary data to this article can be found online at https://doi.org/10.1016/j.scitotenv.2021.152459.

References

Abe, D.S., Adams, D.D., Galli Corina, V.S., Sikar, E., Tundisi, J.G., 2005. Sediment greenhouse gases (methane and carbon dioxide) in the Lobo-Broa Reservoir, São Paulo State, Brazil: concentrations and diffuse emission fluxes for carbon budget considerations. Lakes Reserv. Sci. Policy Manag. Sustain. Use 10, 201–209.

Abril, G., Guerin, F., Richard, S., Delmas, R., Galy-Lacaux, C., Gosse, P., et al., 2005. Carbon dioxide and methane emissions and the carbon budget of a 10-year old tropical reservoir (Petit Saut, French Guiana). Glob. Biogeochem. Cycles 19.

Alicescu, V., 2021. Hydro-Québec, Canada J-P Tournier. Vol. 28. Hydro-Québec & SEBJ, Montréal, Canada Issue 4.

Almeida, R.M., Paranaíba, J.R., Barbosa, Í., Sobek, S., Kosten, S., Linkhorst, A., et al., 2019a. Carbon dioxide emission from drawdown areas of a Brazilian reservoir is linked to surrounding land cover. Aquat. Sci. 81, 68.

Almeida, R.M., Shi, Q., Gomes-Selman, J.M., Wu, X., Xue, Y., Angarita, H., et al., 2019b. Reducing greenhouse gas emissions of Amazon hydropower with strategic dam planning. Nat. Commun. 10, 4281.

Barros, N., Cole, J.J., Tranvik, L.J., Prairie, Y.T., Bastviken, D., Huszar, V.L.M., et al., 2011. Carbon emission from hydroelectric reservoirs linked to reservoir age and latitude. Nat. Geosci. 4, 593–596.

Bastien, J., Demarty, M., Tremblay, A., Gill, R., 2009. Use of automated systems to measure greenhouse gas emissions from reservoirs. Air and Waste Management Association - 1st International Greenhouse Gas Measurement Symposium 2009. 182, pp. 154–159.

Bastien, J., Demarty, M., Tremblay, A., 2011. CO2 and CH4 diffusive and degassing emissions from 2003 to 2009 at Eastmain 1 hydroelectric reservoir, Québec,Canada. Inland Waters 1, 113–123.

Bates, D., Mächler, M., Bolker, B., Walker, S., 2015. Fitting Linear Mixed-effects Models Using lme4. 67, p. 48 2015.

Beaulieu, J.J., McManus, M.G., Nietch, C.T., 2016. Estimates of reservoir methane emissions based on a spatially balanced probabilistic-survey. Limnol. Oceanogr. 61, S27–S40.

Benoit, T., Achraf, E., 2019. Package 'suncalc' Version 0.5.

Bolker, B.M., 2015. Linear and generalized linear mixed models. Ecological Statistics: Contemporary Theory And Application, pp. 309–333.

Chowdhury, T.R., Dick, R.P., 2013. Ecology of aerobic methanotrophs in controlling methane fluxes from wetlands. Appl. Soil Ecol. 65, 8–22.

Conrad, R., 2009. The global methane cycle: recent advances in understanding the microbial processes involved. Environ. Microbiol. Rep. 1, 285–292.

Deemer, B.R., Holgerson, M.A., 2021. Drivers of methane flux differ between lakes and reservoirs, complicating global upscaling efforts. J. Geophys. Res. Biogeosci. 126, e2019JG005600.

Deemer, B.R., Harrison, J.A., Li, S., Beaulieu, J.J., DelSontro, T., Barros, N., et al., 2016. Greenhouse gas emissions from reservoir water surfaces: a new global synthesis. Bioscience 66, 949–964.

DelSontro, Beaulieu J.J., Downing, J.A., 2018. Greenhouse gas emissions from lakes and impoundments: upscaling in the face of global change. Limnol.Oceanogr.Lett. 3, 64–75.

Delsontro, T., McGinnis, D.F., Sobek, S., Ostrovsky, I., Wehrli, B., 2010. Extreme methane emissions from a swiss hydropower reservoir: contribution from bubbling sediments. Environ.Sci.Technol. 44, 2419–2425.

Demarty, M., Bastien, J., Tremblay, A., Hesslein, R.H., Gill, R., 2009. Greenhouse gas emissions from boreal reservoirs in Manitoba and Québec, Canada, measured with automated systems. Environ.Sci.Technol. 43, 8908–8915.

Demarty, M., Bastien, J., Tremblay, A., 2011. Annual follow-up of gross diffusive carbon dioxide and methane emissions from a boreal reservoir and two nearby lakes in Québec, Canada. Biogeosciences 8.

Denfeld, B.A., Lupon, A., Sponseller, R.A., Laudon, H., Karlsson, J., 2020. Heterogeneous CO2 and CH4 patterns across space and time in a small boreal lake. Inland Waters 10, 348–359.

Deshmukh, C., Guérin, F., Vongkhamsao, A., Pighini, S., Oudone, P., Sopraseuth, S., et al., 2018. Carbon dioxide emissions from the flat bottom and shallow Nam Theun 2 Reservoir: drawdown area as a neglected pathway to the atmosphere. Biogeosciences 15, 1775–1794.

Fearnside, P.M., 2006. Greenhouse gas emissions from hydroelectric dams: Reply to Rosa et al. Climatic Change. 75, pp. 103–109.

Flanagan, L.B., Syed, K.H., 2011. Stimulation of both photosynthesis and respiration in response to warmer and drier conditions in a boreal peatland ecosystem. Glob. Chang. Biol. 17, 2271–2287.

Guerin, F., Abril, G., Richard, S., Burban, B., Reynouard, C., Seyler, P., et al., 2006. Methane and carbon dioxide emissions from tropical reservoirs: significance of downstream rivers. Geophys. Res. Lett. 33.

Harrison, J.A., Prairie, Y.T., Mercier-Blais, S., Soued, C., 2021. Year-2020 global distribution and pathways of reservoir methane and carbon dioxide emissions according to the greenhouse gas from reservoirs (G-res) model. Glob. Biogeochem. Cycles 35, e2020GB006888.

Huttunen, J.T., Väisänen, T.S., Hellsten, S.K., Heikkinen, M., Nykänen, H., Jungner, H., et al., 2002. Fluxes of CH4, CO2, and N2O in hydroelectric reservoirs Lokka and Porttipahta in the northern boreal zone in Finland. Glob. Biogeochem. Cycles 16.

Hydro-Québec, 2008. Romaine Environmental Impact Report. Hydro-Québec Production.

IPCC, 2021. Climate change 2021: the physical science basis. Contribution of Working Group I to the Sixth Assessment Report of the Intergovernmental Panel on Climate Change. Cambridge University Press In Press.

Johnson, M.S., Matthews, E., Bastviken, D., Deemer, B., Du, J., Genovese, V., 2021. Spatiotemporal methane emission from global reservoirs. J. Geophys. Res. Biogeosci. 126, e2021JG006305.

Keller, P.S., Marcé, R., Obrador, B., Koschorreck, M., 2021. Global carbon budget of reservoirs is overturned by the quantification of drawdown areas. Nat. Geosci. 14, 402–408.

Kemenes, A., Forsberg, B.R., Melack, J.M., 2007. Methane release below a tropical hydroelectric dam. Geophys. Res. Lett. 34.

Kling, G.W., Kipphut, G.W., Miller, M.C., 1991. Arctic lakes and streams as gas conduits to the atmosphere: implications for tundra carbon budgets. Science 251, 298.

Kosten, S., van den Berg, S., Mendonça, R., Paranaíba, J.R., Roland, F., Sobek, S., et al., 2018. Extreme drought boosts CO2 and CH4 emissions from reservoir drawdown areas. Inland Waters 8, 329–340.

Lima, I.B.T., 2005. Biogeochemical distinction of methane releases from two Amazon hydroreservoirs. Chemosphere 59, 1697–1702.

Liu, L., Yang, Z., Delwiche, K., Long, L., Liu, J., Liu, D., et al., 2020. Spatial and temporal variability of methane emissions from cascading reservoirs in the Upper Mekong River. Water Res. 186, 116319.

Loken, L.C., Crawford, J.T., Schramm, P.J., Stadler, P., Desai, A.R., Stanley, E.H., 2019. Large spatial and temporal variability of carbon dioxide and methane in a eutrophic lake. J. Geophys.Res.Biogeosci. 124, 2248–2266.

Maeck, A., DelSontro, T., McGinnis, D.F., Fischer, H., Flury, S., Schmidt, M., et al., 2013. Sediment trapping by dams creates methane emission hot spots. Environ.Sci.Technol. 47, 8130–8137.

McClure, R.P., Lofton, M.E., Chen, S., Krueger, K.M., Little, J.C., Carey, C.C., 2020. The magnitude and drivers of methane ebullition and diffusion vary on a longitudinal gradient in a small freshwater reservoir. J. Geophys. Res. Biogeosci. 125, e2019JG005205.

Mendonça, R., Barros, N., Vidal, L., Pacheco, F., Kosten, S., Roland, F., 2012. Greenhouse Gas Emissions From Hydroelectric Reservoirs: What Knowledge Do We Have And What is Lacking?

Morales-Pineda, M., Cózar, A., Laiz, I., Úbeda, B., Gálvez, J.Á., 2014. Daily, biweekly, and seasonal temporal scales of pCO2 variability in two stratified Mediterranean reservoirs. J. Geophys.Res.: Biogeosci. 119, 509–520.

Okuku, E.O., Bouillon, S., Tole, M., Borges, A.V., 2019. Diffusive emissions of methane and nitrous oxide from a cascade of tropical hydropower reservoirs in Kenya. Lakes Reserv. Res. Manag. 24, 127–135.

Paranaíba, J.R., Barros, N., Mendonça, R., Linkhorst, A., Isidorova, A., Roland, F., et al., 2018. Spatially resolved measurements of CO2 and CH4 concentration and gas-exchange velocity highly influence carbon-emission estimates of reservoirs. Environ.Sci.Technol. 52, 607–615.

Prairie, Y.T., Alm, J., Beaulieu, J., Barros, N., Battin, T., Cole, J., et al., 2018. Greenhouse gas emissions from freshwater reservoirs: what does the atmosphere see? Ecosystems 21, 1058–1071.

Prairie, Y.T., Mercier-Blais, S., Harrison, J.A., Soued, C., Giorgio, Pd., Harby, A., et al., 2021. A new modelling framework to assess biogenic GHG emissions from reservoirs: the G-res tool. Environ. Model Softw. 143, 105117.

Roland, F., Vidal, L.O., Pacheco, F.S., Barros, N.O., Assireu, A., Ometto, J.P.H.B., et al., 2010. Variability of carbon dioxide flux from tropical (Cerrado) hydroelectric reservoirs. Aquat. Sci. 72, 283–293.

Rosa, L.P., Dos Santos, M.A., Matvienko, B., Sikar, E., Dos Santos, E.O., 2006. Scientific errors in the fearnside comments on greenhouse gas emissions (GHG) from hydroelectric dams and response to his political claiming. Clim. Chang. 75, 91–102.

Rosentreter, J.A., Borges, A.V., Deemer, B.R., Holgerson, M.A., Liu, S., Song, C., et al., 2021. Half of global methane emissions come from highly variable aquatic ecosystem sources. Nat. Geosci. 14, 225–230.

Rudd, J.W.M., Hecky, R.E., Harris, R., Kelly, C.A., 1993. Are hydroelectric reservoirs significant sources of greenhouse gases. Ambio 22 (4), 246–248.

Sand-Jensen, K., Pedersen, N.L., Sondergaard, M., 2007. Bacterial metabolism in small temperate streams under contemporary and future climates. Freshw. Biol. 52, 2340–2353.

Shi, W., Chen, Q., Yi, Q., Yu, J., Ji, Y., Hu, L., et al., 2017. Carbon emission from cascade reservoirs: spatial heterogeneity and mechanisms. Environ.Sci.Technol. 51, 12175–12181.

Sobek, S., Tranvik, L.J., Cole, J.J., 2005. Temperature independence of carbon dioxide supersaturation in global lakes. Glob. Biogeochem. Cycles 19.

Sobek, S., DelSontro, T., Wongfun, N., Wehrli, B., 2012. Extreme organic carbon burial fuels intense methane bubbling in a temperate reservoir. Geophys. Res. Lett. 39.

Soued, C., Prairie, Y.T., 2020. The carbon footprint of a Malaysian tropical reservoir: measured versus modelled estimates highlight the underestimated key role of downstream processes. Biogeosciences 17, 515–527.

Team RC, 2018. R: A Language And Environment for Statistical Computing [Google Scholar].

Teodoru, Prairie, Y., del Giorgio, P., 2011. Spatial heterogeneity of surface CO2 fluxes in a newly created Eastmain-1 reservoir in Northern Quebec, Canada. Ecosystems 14, 28–46.

Teodoru, C.R., Bastien, J., Bonneville, M.-C., del Giorgio, P.A., Demarty, M., Garneau, M., et al., 2012b. The net carbon footprint of a newly created boreal hydroelectric reservoir. Glob. Biogeochem. Cycles 26.

Teodoru, Bastien J., Bonneville, M.-C., del Giorgio, P.A., Demarty, M., Garneau, M., et al., 2012;;. The net carbon footprint of a newly created boreal hydroelectric reservoir. Glob. Biogeochem. Cycles 26.

Thauer, R.K., Kaster, A.-K., Seedorf, H., Buckel, W., Hedderich, R., 2008. Methanogenic archaea: ecologically relevant differences in energy conservation. Nat. Rev. Microbiol. 6, 579–591.

Therneau, T., Atkinson, B., Ripley, B., 2019. rpart: Recursive Partitioning And Regression Trees. R Package Version 4.1–13. 2019.

Venkiteswaran, J.J., Schiff, S.L., St. Louis, V.L., CJD, Matthews, Boudreau, N.M., Joyce, E.M., 2013. Processes affecting greenhouse gas production in experimental boreal reservoirs. Glob. Biogeochem. Cycles 27, 567–577.

Wang, F., Wang, B., Liu, C.-Q., Wang, Y., Guan, J., Liu, X., et al., 2011. Carbon dioxide emission from surface water in cascade reservoirs–river system on the Maotiao River, southwest of China. Atmos. Environ. 45, 3827–3834.

Wang, F., Cao, M., Wang, B., Fu, J., Luo, W., Ma, J., 2015. Seasonal variation of CO2 diffusion flux from a large subtropical reservoir in East China. Atmos. Environ. 103, 129–137.

Wang, W., Li, S.-L., Zhong, J., Wang, L., Yang, H., Xiao, H., et al., 2021. CO2 emissions from karst cascade hydropower reservoirs: mechanisms and reservoir effect. Environ. Res. Lett. 16, 044013.

Weiss, R.F., 1970. The solubility of nitrogen, oxygen and argon in water and seawater. Deep-Sea Res. Oceanogr. Abstr. 17, 721–735.

Wiesenburg, D.A., Guinasso, N.L., 1979. Equilibrium solubilities of methane, carbon monoxide, and hydrogen in water and sea water. J. Chem. Eng. Data 24, 356–360.

Wik, M., Varner, R.K., Anthony, K.W., MacIntyre, S., Bastviken, D., 2016. Climate-sensitive northern lakes and ponds are critical components of methane release. Nat. Geosci. 9, 99–105.

Yvon-Durocher, G., Allen, A.P., Bastviken, D., Conrad, R., Gudasz, C., St-Pierre, A., et al., 2014. Methane fluxes show consistent temperature dependence across microbial to ecosystem scales. Nature 507, 488.